Nanoscale

PAPER

View Article Online
View Journal | View Issue

Cite this: *Nanoscale*, 2025, **17**, 14408

Atomically precise large-sized $Au_n(SR)_m$ nanoclusters and scaling relationships among size, bandgap and excited-state lifetime†

Xiangsha Du,‡[a] Tatsuya Higaki, ‡[a] Hedi Ma,‡[b] Xinwen Zhang,‡[c] Gangli Wang, *[b] He Wang *[c] and Rongchao Jin *[a]

The synthesis of atomically precise, large-sized $Au_n(SR)_m$ nanoclusters (SR = thiolate) with n of 100 or more atoms has long been a challenge. In this work, we report the synthesis of $Au_{100}(Napt)_{42}$ and $Au_{102}(IPBT)_{44}$ nanoclusters (where Napt stands for 1-naphthalenethiolate and IPBT for 4-isopropylbenzenethiolate). Their optical absorption, single-electron charging, and femtosecond electron dynamics are investigated. Both $Au_{100}(Napt)_{42}$ and $Au_{102}(IPBT)_{44}$ exhibit multiple discrete absorption bands in their optical spectra owing to a quantized electronic structure in ultrasmall metal nanoclusters. Electrochemical analysis determines the precise HOMO–LUMO gaps of $Au_{100}(Napt)_{42}$ and $Au_{102}(IPBT)_{44}$ by single-electron charging. The electronic excited-state lifetimes of $Au_{100}(Napt)_{42}$ and $Au_{102}(IPBT)_{44}$ are determined by femtosecond transient absorption spectroscopy. The scaling relationship between the E_g and size (n) and the relationship of the excited state lifetime *versus* the E_g of large-sized $Au_n(SR)_m$ are discussed. The findings provide a fundamental understanding of large-sized metal nanoclusters, which will benefit their future applications in optics, electronics, and other fields.

Received 25th March 2025,
Accepted 8th May 2025

DOI: 10.1039/d5nr01244a

rsc.li/nanoscale

Introduction

When the size of metal nanoparticles is reduced to ~2.2 nanometers, distinct quantum confinement effects come into play, manifested in the emergence of a sizable HOMO–LUMO gap (E_g) and the disappearance of plasmon resonance.[1–3] Fundamental studies of the electronic and optical properties of such quantum-sized nanoclusters (NCs) require precise size control at the single-atom level.[4–8] In recent years, breakthroughs in the synthesis have led to the establishment of a library of atomically precise $Au_n(SR)_m$ NCs.[9] These Au NCs can be protected by ligands such as thiolate,[1] phosphine,[2] alkynyl,[6,10] N-heterocyclic carbene,[7,11] and halide.[12] The structural diversity of the Au kernel and Au–ligand interface, as well as the organic outer shell, provides great tunability of the functionality of NCs for diverse applications.[13–18]

In the quantum-size regime (*e.g.*, tens to hundreds of atoms per core), the material properties of gold NCs become very sensitive even to a small variation; for example, a single-atom variation can trigger structural transformation, and single-atom doping may induce significant changes to the optical absorption, photoluminescence, catalytic activity, and magnetic properties.[19–21] The same adamantanethiolate-protected $Au_{21}(SR)_{15}$, $Au_{22}(SR)_{16}$, $Au_{22}Cd(SR)_{16}$, and $Au_{24}(SR)_{16}$ series offers a neat platform for atom-by-atom evolution of small-sized NCs.[22] Structurally, a single cadmium addition to $Au_{22}(SR)_{16}$ induces a surface reconstruction in $Au_{22}Cd_1(SR)_{16}$ as well as a kernel reconstruction from the Au_{10} bioctahedron in $Au_{22}(SR)_{16}$ to the Au_{13} cuboctahedron in $Au_{22}Cd_1(SR)_{16}$.[22] The addition of metal atoms to the NC in an atom-by-atom manner also causes dramatic changes to the optical absorption, reflected in the distinct color changes to the NCs.[22] Such a high sensitivity of the structural and optical properties to single-atom variations is due to the strong quantum confinement effect in small NCs. In addition to the optical effects, recent work on various crystalline phases of Au NCs also found that the electronic excited-state relaxation can be drastically varied by the metal core's phase,[23] with the hexagonal close-packed $Au_{30}(SR)_{18}$ and body-centered cubic $Au_{38}S_2(SR)_{20}$ NCs protected by the same type of ligand showing a three-orders-of-magnitude variation of the photoexcited carrier lifetime. On the other hand, for larger sized $Au_n(SR)_m$ NCs, the sensitivity of pro-

---

[a] Department of Chemistry, Carnegie Mellon University, Pittsburgh, Pennsylvania 15213, USA. E-mail: rongchao@andrew.cmu.edu
[b] Department of Chemistry, Georgia State University, Atlanta, Georgia 30302, USA. E-mail: glwang@gsu.edu
[c] Department of Physics, University of Miami, Coral Gables, Florida 33146, USA. E-mail: hewang@miami.edu

† Electronic supplementary information (ESI) available. See DOI: https://doi.org/10.1039/d5nr01244a

‡ These authors contributed equally.

perties to the variation in size (n) remains less studied, as more efforts on the synthesis of large-sized NCs are still needed.

In the investigation of how the optical properties of gold NCs evolve with increasing size (n, the number of gold atoms), Negishi *et al.* previously reported a series of $Au_n(SC_{12})_m$ NCs with n ranging from 38 to ∼520, in which the critical region—where a molecule-like electronic structure and a non-bulk geometric structure emerge—was determined to be between Au_{144} and Au_{187}.[24] Higaki *et al.* determined the transition from non-metallic Au_{246} to metallic Au_{279}.[25,26] When taking the shape factor into consideration, Pei's group carried out theoretical work and reported that $Au_{264}(SH)_{96}$ is a critical size for the transition in cuboidal NCs.[27] Zhou *et al.* drew a grand picture of the three-stage evolution from non-scalable to scalable optical properties of $Au_n(SR)_m$ NCs.[28] Nevertheless, the large-sized NCs with $n \geq 100$ atoms still remain scarce and synthetically challenging. To further investigate the scaling relationship of the optical and electronic properties with the number of Au atoms in the NCs, more large-sized NCs should be synthesized and their electronic and optical properties should be investigated.

Herein, we report the synthesis, optical absorption and electronic properties of $Au_{100}(Napt)_{42}$ and $Au_{102}(IPBT)_{44}$ NCs. These NCs exhibit ultrasmall gaps (E_g < 0.5 eV), and precise determination of such gaps is not trivial.[2] Their steady-state and transient optical absorption properties are studied. Furthermore, we summarize the scaling relationships of the gap E_g *vs.* size (n), as well as the carrier lifetime *vs.* E_g in the large-size regime. The findings of this work provide a deeper understanding of the size evolution behavior of the electronic properties of NCs in the large-size regime.

Results and discussion

Synthesis and characterization of $Au_{100}(Napt)_{42}$ and $Au_{102}(IPBT)_{44}$

$Au_{100}(Napt)_{42}$ (Napt = 1-naphthalenethiolate) was prepared by a ligand-exchange reaction from polydispersed $Au_x(2,4\text{-DMBT})_y$ nanoclusters (2,4-DMBT = 2,4-dimethylbenzenethiol) at 80 °C overnight; of note, the $Au_x(2,4\text{-DMBT})_y$ crude product was prepared by $NaBH_4$ reduction of $HAuCl_4·3H_2O$ in a two-phase solution (toluene/water). Separation of $Au_{100}(Napt)_{42}$ from side products was achieved by thin-layer chromatography (TLC); further synthetic details are provided in the ESI.† The high purity and molecular formula of $Au_{100}(Napt)_{42}$ are confirmed by matrix-assisted laser desorption ionization (MALDI) and electrospray ionization (ESI) mass spectrometry analyses. As can be seen in Fig. 1(a), the MALDI spectrum shows a very narrow peak at ∼25 kDa for $Au_{100}(Napt)_{42}$, indicating its high purity. Its precise mass was determined by ESI-MS (Fig. 1a, inset). A dominant peak of the molecular ion at *m*/*z* 8794.09 (M^{3+}) was observed, along with a minor peak at 13 192.75 (not shown) corresponding to the 2+ ion. These ions are formed under the ESI conditions, as the native state of the NC is charge neutral. Both peaks match well with the calculated mass of $Au_{100}(Napt)_{42}$ (FW = 26 384.20 Da). The UV–vis spectrum of $Au_{100}(Napt)_{42}$ shows multiple absorption bands at 430, 520, 610, and 730 nm in the visible range (Fig. 1b) due to ultrasmall size-induced quantization of the electronic structure, as opposed to the quasi-continuous conduction band in metallic-state nanoparticles. All these bands are highly congested, which is typical of large-sized NCs due to their much denser electronic states compared to small sized NCs such as $Au_{25}(SR)_{18}$, where the peaks are well separated.[9] The highly structured, molecular-like optical features in gold nanoclusters often indicate high purity, as size-mixed nanoclusters readily wash out such features and give rise to a featureless, decay-like spectrum.

We next discuss the case of $Au_{102}(IPBT)_{44}$, which was synthesized by a two-step, size-focusing method. Briefly, a polydispersed $Au_x(IPBT)_y$ mixture was first obtained by the reactions of $HAuCl_4·3H_2O$ with 4-isopropylbenzenethiol (IPBT) and reduction by $NaBH_4$. Further thermal etching of the poly-dispersed $Au_x(IPBT)_y$ was conducted in toluene with 0.5 mL IPBT at 80 °C. After washing with methanol, pure $Au_{102}(IPBT)_{44}$ was collected. In MALDI-MS analysis, a single peak was observed at

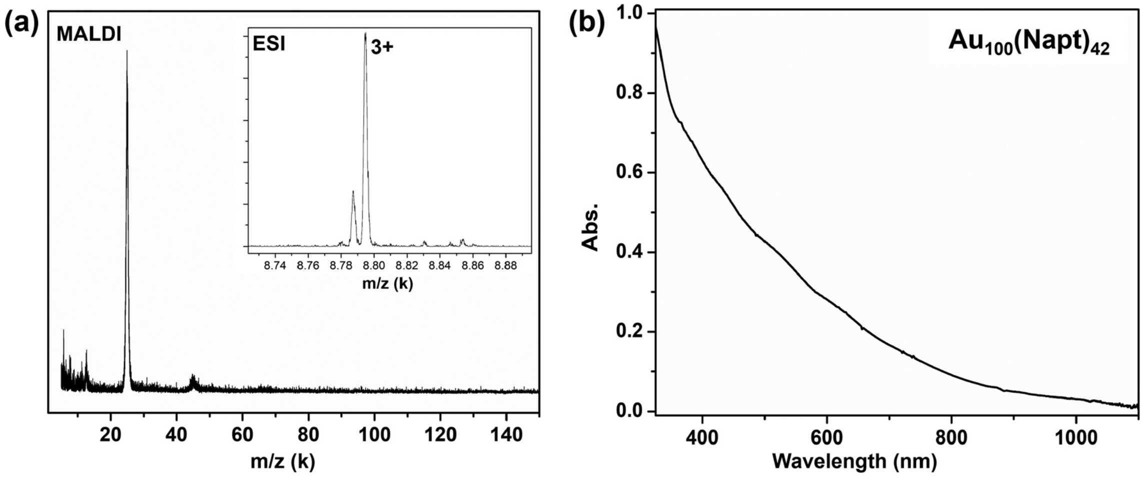

Fig. 1 (a) MALDI and ESI (inset) mass spectra of $Au_{100}(Napt)_{42}$; (b) absorption spectrum of $Au_{100}(Napt)_{42}$.

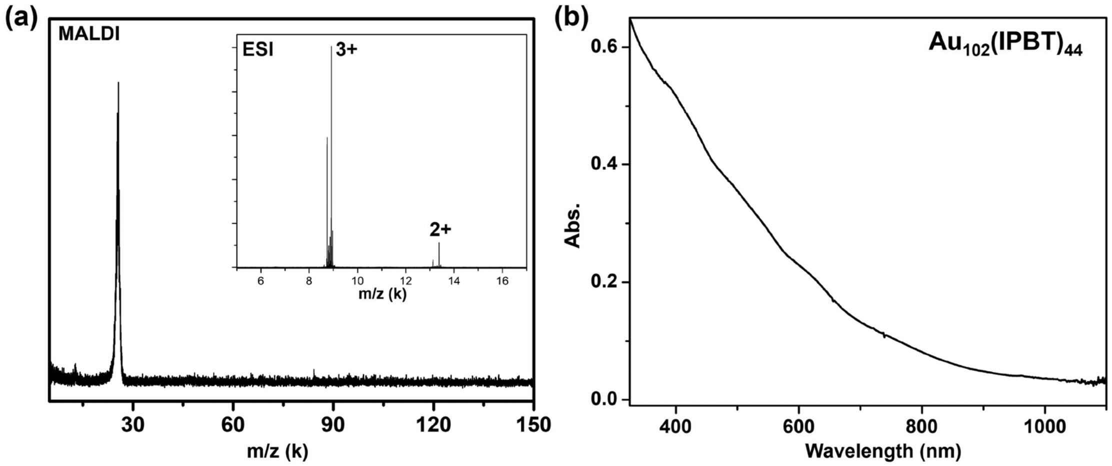

Fig. 2 (a) MALDI and ESI (inset) mass spectra of $Au_{102}(IPBT)_{44}$; (b) absorption spectrum of $Au_{102}(IPBT)_{44}$.

~25 kDa (Fig. 2a), demonstrating the high purity of the sample. The ESI spectrum gives two sets of peaks at *m*/*z* 8915.59 (3+) and 13 373.20 (2+), corresponding to the 3+ and 2+ ions, respectively. Both peaks are consistent with the expected formula weight of $Au_{102}(IPBT)_{44}$ (FW = 26 746.38 Da). Of note, the slight fragmentation within each set (Fig. 2a inset) is caused by the subtraction or addition of one IPBT ligand. The optical absorption spectrum of $Au_{102}(IPBT)_{44}$ shows peaks at 420, 505, 600, and 730 nm (Fig. 2b), which are comparable to the bands of $Au_{100}(Napt)_{42}$, indicating an intrinsic relationship (see below), in particular, given the fact that these two NCs differ by only two gold atoms and two ligands.

Structural insights

The highly structured optical absorption spectra of $Au_n(SR)_m$ NCs reflect the metal core structures and can indeed serve as "fingerprints".[9] We find that the optical spectra of both $Au_{100}(Napt)_{42}$ and $Au_{102}(IPBT)_{44}$ are quite similar to those of previously reported $Au_{102}(p\text{-MBA})_{44}$ and $Au_{103}S_2(Napt)_{41}$ (Fig. S1†) having solved structures.[29,30] This can be explained by the fact that all these four NCs (charge-neutral) possess the same number of nominal free-electron count, *i.e.*, 58e, *e.g.*, 100 (Au $6s^1$) − 42 (monovalent SR ligand) = 58e. It should be noted that the S species in the $Au_{103}S_2(Napt)_{41}$ nanocluster localizes two electrons per S atom due to its divalent nature (S^{2-}), so the free electron number = 103 − 2 × 2 − 41 = 58e. It is worth noting that the $Au_{102}(IPBT)_{44}$ nanocluster from the current work shares the same number of gold atoms and ligands (though hydrophobic) with the previously reported aqueous phase $Au_{102}(p\text{-MBA})_{44}$ (where *p*-MBA = SPh-*p*-COOH), with the only difference being in the *para*-substitution on the benzene ring (*i.e.*, isopropyl *vs.* –COOH). Based on the empirical rule that the kernel structure plays a decisive role in the optical absorption spectra,[9] plus the fact that the four abovementioned NCs share the same 58e count, we deduce that $Au_{102}(IPBT)_{44}$ should have the same Au_{79} Marks decahedral kernel, *i.e.*, a shell-by-shell $Au_7@Au_{32}@Au_{40}$ arrangement, and the surface should be composed of 19 monomeric (SR–Au–SR) and two dimeric (SR–Au–SR–Au–SR) staple-like motifs as in the structure of its aqueous soluble $Au_{102}(p\text{-MBA})_{44}$ counterpart.[29] With respect to $Au_{100}(Napt)_{42}$, we also deduce that the same Au_{79} decahedron should be adopted, but the surface should comprise 21 monomeric (SR–Au–SR) staple motifs protecting the Au_{79} kernel, similar to the pair of $Au_{102}(p\text{-MBA})_{44}$ and $Au_{103}S_2(Napt)_{41}$ NCs, which share the same Au_{79} kernel but slightly different surface motifs.[29,30]

Compared to the previously reported aqueous $Au_{102}(p\text{-MBA})_{44}$,[29] the attainment of organic soluble $Au_{102}(IPBT)_{44}$ in the current work allows for a precise determination of E_g and a detailed study on the single-electron charging energy, which was previously inaccessible with the aqueous $Au_{102}(p\text{-MBA})_{44}$ (*vide infra*).

HOMO–LUMO gap determination and the scaling relationship with size

The 58e system with close sizes (*n* = 100, 102 and 103) and various ligands is a great platform for a comparative study of their electronic properties. Here, we carried out further electrochemical measurements. Differential pulse voltammetry (DPV) analysis indicates that both $Au_{100}(Napt)_{42}$ and $Au_{102}(IPBT)_{44}$ exhibit discrete electronic energy levels and rich charge states (Fig. 3). Following a meticulous method established by Wang and coworkers,[31] the E_g of $Au_{100}(Napt)_{42}$ was deduced to be 0.40 eV from the electrochemical gap between the first oxidation and the first reduction potentials after subtracting the charging energy (*i.e.*, 0.61_2–0.21_6 = 0.40 eV; the subscripts indicate single-meV accuracy[31]). Similarly, the E_g of $Au_{102}(IPBT)_{44}$ is 0.33 eV (*i.e.*, 0.57_2–0.24_4 = 0.33 eV). The gaps of these two 58e NCs are similar to those of $Au_{102}(p\text{-MBA})_{44}$ (0.45 eV)[29] and $Au_{103}S_2(Napt)_{41}$ (0.38 eV).[30] The similar E_g values of these four 58e NCs support the abovementioned rationale for using the same Au_{79} kernel.

It is worth comparing the determined E_g of Au_{100} and Au_{102} NCs (quasi-spherical) with other NCs of slightly smaller or larger sizes, such as $Au_{92}(TBBT)_{44}$[32] and $Au_{99}(SR)_{42}$,[33,34] and

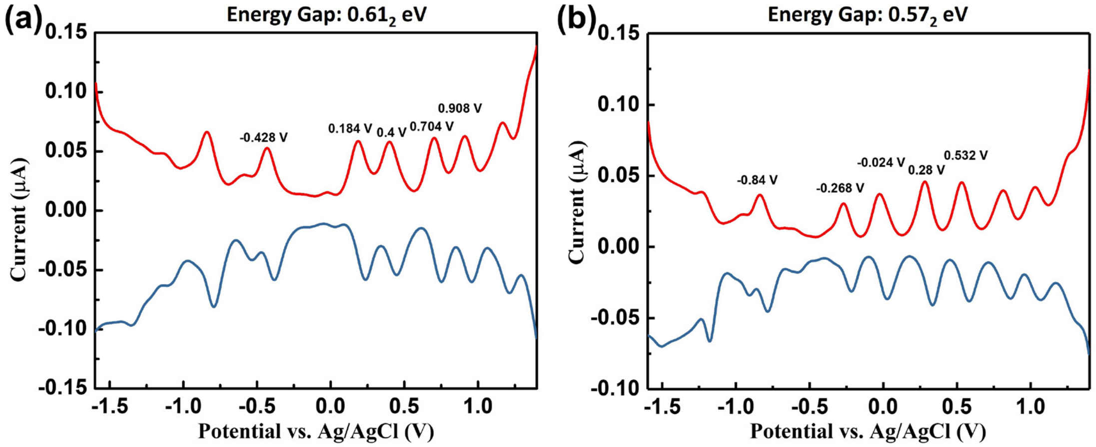

$Au_{100}(Napt)_{42}$ $Au_{102}(IPBT)_{44}$

Fig. 3 Differential pulse voltammograms of (a) $Au_{100}(Napt)_{42}$ and (b) $Au_{102}(IPBT)_{44}$. The gaps of 0.612 and 0.572 eV are without subtraction of charging energy.

two rod-shaped NCs of $Au_{96}(PET)_{68}$ and $Au_{114}(PET)_{80}$.[35] Fig. 4 shows a plot of E_g *versus* the number of gold atoms (n) in the size range between 92 and 114, as well as those with larger sizes, including $Au_{130}(SR)_{50}$ (various types of ligands),[36–39] $Au_{133}(SR)_{52}$,[40,41] and $Au_{144}(SR)_{60}$.[42–44] One can see that the spherical (or nearly spherical) NCs exhibit a trend (Fig. 4, the black solid line is a guide). Interestingly, their E_g is generally smaller than that of the rod-shaped $Au_{96}(PET)_{68}$ and $Au_{114}(PET)_{80}$ by ∼0.27 eV (*i.e.*, the gap between the top and lower lines, Fig. 4) at comparable sizes. We attribute this to two factors: (i) the shape-induced quantum effect on the electronic structure, *i.e.*, the lower symmetry of quantum rods[35] leads to a stronger quantum confinement effect in the smaller dimension of the rods, and (ii) the higher ligand-to-gold ratio in rod-shaped NCs, *e.g.*, the $Au_{96}(PET)_{68}$ rods possess many more ligands (∼43% higher) than $Au_{100}(Napt)_{42}$ and $Au_{102}(IPBT)_{44}$. The latter factor is expected to enlarge the E_g because more valence electrons (6s of gold atoms) are localized in the covalent bonds of Au–SR motifs.

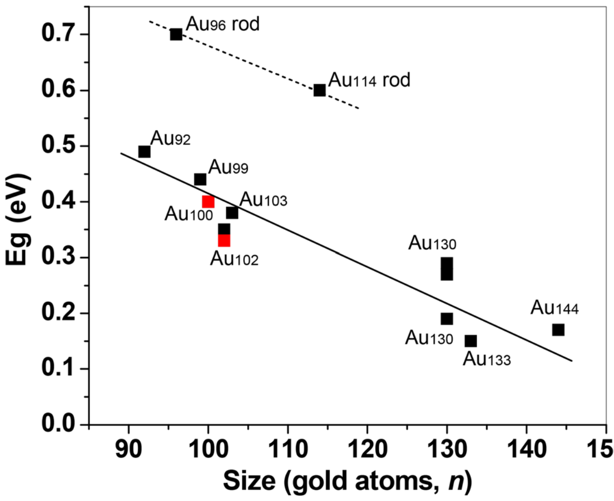

Fig. 4 Scaling relationship between the E_g of large-sized $Au_n(SR)_m$ NCs and the number of gold atoms (n).

Ultrafast electron dynamics in Au_{100} and Au_{102} NCs

Gold NCs with 100 atoms or more have ultrasmall energy gaps (E_g < 0.5 eV), which are hard to reach for other molecular materials; thus, such NCs are quite unique and worthy of investigation due to their electron dynamics. Here, we probe the excited-state dynamics of $Au_{100}(Napt)_{42}$ and $Au_{102}(IPBT)_{44}$ by performing femtosecond transient absorption (fs-TA for short) measurements. After photoexcitation at 400 nm, the NCs exhibit significant fast and slow decays in the relaxation process (Fig. 5a and b). $Au_{100}(Napt)_{42}$ and $Au_{102}(IPBT)_{44}$ show very similar TA spectra and relaxation dynamics, which further indicates that they should share a similar atomic structure (Au_{79} kernel). Specifically, a distinct ground-state bleaching (GSB) signal is seen at ∼525 nm, which matches with the ground state absorption band in both NCs. Strong excited-state absorption (ESA) signals are observed at 580 and 675 nm. Overall, the similar GSB and ESA signals for both NCs also indicate their similar electronic structures.

Global analysis on the fs-TA data gives three decay components for both NCs (Fig. 5c and d). The fast relaxation can be fitted by two processes: the <1 ps process is assigned to the relaxation from the higher excited state to the lower excited state, while the few-picosecond process should be considered as the energy rearrangement process around the lowest excited state (ESI Fig. S2†). The slow process takes 266 ps for $Au_{100}(Napt)_{42}$ and 466 ps for $Au_{102}(IPBT)_{44}$, which are the relaxation from the lowest excited state to the ground state (*i.e.* exciton recombination). Based on the above observations, we can deduce that upon photoexcitation, transitions from the ground state to the excited state occur predominantly through core-based orbitals, and the excited core then relaxes *via* core phonons and hence exhibits similar relaxation dynamics.

Among the 58e NCs (organic soluble ones, including $Au_{100}(Napt)_{42}$ (E_g = 0.40 eV), $Au_{102}(IPBT)_{44}$ (E_g = 0.33 eV), and

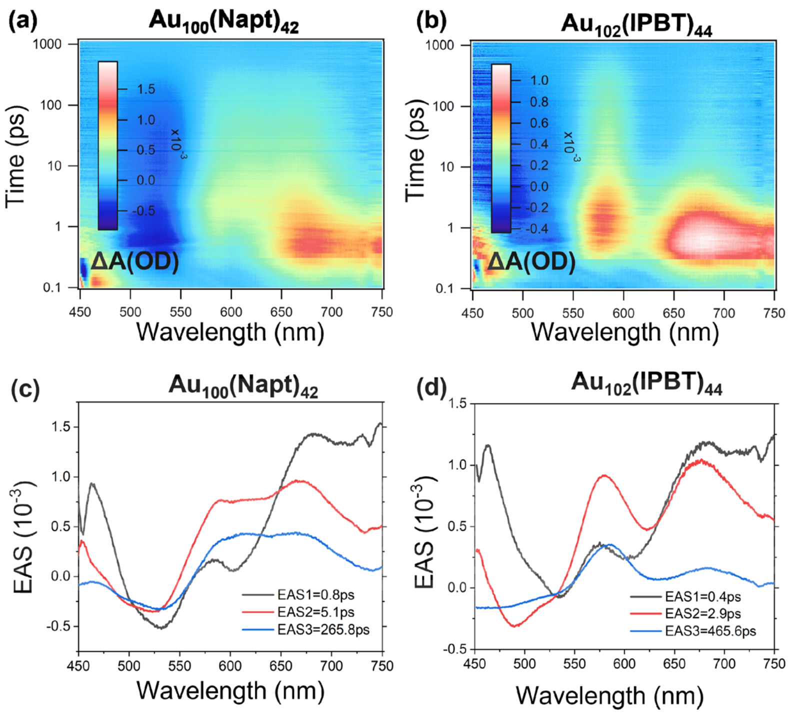

Fig. 5 Transient absorption data map of (a) $Au_{100}(Napt)_{42}$ and (b) $Au_{102}(IPBT)_{44}$ pumped at 400 nm. Evolution associated spectra (EAS) obtained from global fitting of (c) $Au_{100}(Napt)_{42}$ and (d) $Au_{102}(IPBT)_{44}$.

$Au_{103}S_2(Napt)_{41}$ (E_g = 0.4 eV)), a variation of ∼1.8 times (266 *vs.* 466 ps) can be seen in their excited-state lifetimes (ESI Fig. S3†). This is attributed to the surface effect because the excited state relaxation also involves the surface, while the E_g value and optical absorption peaks are primarily dictated by the kernel. When compared to the water phase $Au_{102}(p\text{-MBA})_{44}$ (E_g = 0.45 eV), a 10-time increase in the excited lifetime is observed in $Au_{102}(p\text{-MBA})_{44}$ (ESI Fig. S3†). Such a large effect was also found in the case of organic soluble $Au_{130}(SR)_{50}$ *versus* water soluble $Au_{130}(SR)_{50}$.[37,38] This distinct difference may be caused by the –COOH perturbation to the surface and/or the hydrogen-bonding effect in aqueous NCs.

Scaling relationship of the excited state lifetime with the energy gap

We further discuss the scaling relationship of the excited-state lifetime (τ) with E_g for large-sized $Au_n(SR)_m$ NCs. Here, we focus on (quasi)spherical NCs since more sizes have become available.[2] The lifetimes of $Au_{100}(Napt)_{42}$ and $Au_{102}(IPBT)_{44}$ are much higher than that of the well-known $Au_{144}(SR)_{60}$ (a few ps)[42–44] due to their E_g difference as well as the ligand effects. Our results suggest that when E_g decreases (*i.e.*, approaching the metallic state), the ratio of the fast decay process (on the ps scale) increases in the whole decay process in large-sized NCs such as Au_{130}, Au_{133}, Au_{144} and Au_{246} NCs,[28] which may be ascribed to the difficulty in separation between the fast decay (the relaxation from the higher excited state to the lowest excited state) and slow decay (the relaxation from the lowest excited state to the ground state) when the energy gap is so small. Thus, the excited-state relaxation cannot be treated as a sequential model since there is no population accumulation in the lower excited state for those Au NCs with very small E_g. By fitting the band gaps and excited-state lifetimes of $Au_{100}(Napt)_{42}$, $Au_{102}(IPBT)_{44}$ and other large-sized NCs,[28] we observed a quantitative relationship in which the excited-state lifetimes of Au NCs decrease exponentially with the energy gaps (ESI Fig. S4a†). Here, we fit the data with the energy gap law,

$$k_{nr} = Ae^{-\gamma E_g/\hbar\omega} \tag{1}$$

where k_{nr} is the non-radiative recombination rate, γ is a molecular parameter, and ω is the highest vibrational frequency involved in non-radiative decay. In large-sized NCs (n > 100), photoluminescence is no longer observable; thus, the electron relaxation dynamics is dominated by the non-radiative decay. Accordingly, k_{nr} can be obtained by the inverse of the excited-state lifetime ($1/\tau$) from fs-TA measurements. Using the linear form of eqn (1),

$$\ln k_{nr} = \ln A - \frac{\gamma}{\hbar\omega}E_g \tag{2}$$

we obtained a good linear relationship between $\ln k_{nr}$ and E_g (Fig. S4b†), with the fitted intercept ($\ln A$) being 27.5 and the slope ($-\gamma/\hbar\omega$) being −15 eV^{-1}.

Conclusions

In summary, we devised synthetic routes for two large-sized nanoclusters $Au_{100}(Napt)_{42}$ and $Au_{102}(IPBT)_{44}$ and characterized their optical and electronic properties. Together with $Au_{102}(p\text{-MBA})_{44}$ and $Au_{103}S_2(Napt)_{41}$, a family of four 58e NCs is formed, which allows us to compare their atomic and electronic structures, as well as the electron relaxation dynamics. For the atomic structure, the two new NCs are rationalized to possess the same Au_{79} decahedral kernel as that observed in the crystallographically characterized $Au_{102}(p\text{-MBA})_{44}$ and $Au_{103}S_2(Napt)_{41}$ NCs, evidenced by the similarity in their steady-state absorption and transient absorption spectral features (*e.g.*, common GSB signals at 525 nm and ESA signals at 580 and 675 nm), as well as comparable ultrafast dynamics. The determination of ultrasmall HOMO–LUMO gaps of $Au_{100}(Napt)_{42}$ and $Au_{102}(IPBT)_{44}$ is nontrivial but is successfully done by meticulous DPV analysis. The E_g values (~0.4 eV) of $Au_{100}(Napt)_{42}$ and $Au_{102}(IPBT)_{44}$ are similar to those of their crystallographically characterized counterparts, indicating the decisive role of the kernel in the ground-state electronic properties, while the excited-state dynamics involves both the kernel and surface (*i.e.*, the ligand dependence). Finally, extensive analyses done by summarizing the NCs from $Au_{92}(SR)_{44}$ to $Au_{279}(SR)_{84}$ give rise to the scaling relationships between the E_g and size (n), as well as the relationship between the excited-state lifetime and E_g, from which we identified a strong shape effect on E_g and also strong nonradiative decay. Such findings greatly deepen our fundamental understanding of the optical and electronic properties of $Au_n(SR)_m$ NCs in the large-size regime, which will benefit the future development of applications of such atomically precise materials.

Data availability

All the data are available and reported in the manuscript and its ESI.†

Conflicts of interest

The authors have no conflicts of interest to declare.

Acknowledgements

We thank Dr Meng Zhou for helpful discussions. This material is based upon the work supported as part of the Atomic-C2E project by the U.S. Department of Energy, Office of Science under award number DE-SC-0024716. H. W. acknowledges financial support by the Air Force Office of Scientific Research (AFOSR) under award number FA9550-21-1-0192.

References

1 H. Qian, M. Zhu, Z. Wu and R. Jin, *Acc. Chem. Res.*, 2012, **45**, 1470–1479.

2 T. Kawawaki and Y. Negishi, *Dalton Trans.*, 2023, **52**, 15152–15167.

3 M. Zhou, C. Zeng, Y. Song, J. W. Padelford, G. Wang, M. Y. Sfeir, T. Higaki and R. Jin, *Angew. Chem., Int. Ed.*, 2017, **56**, 16257–16261.

4 Y. Li, M. Zhou, Y. Song, T. Higaki, H. Wang and R. Jin, *Nature*, 2021, **594**, 380–384.

5 N. Yan, N. Xia, L. Liao, M. Zhu, F. Jin, R. Jin and Z. Wu, *Sci. Adv.*, 2018, **4**, eaat7259.

6 J.-Q. Wang, S. Shi, R.-L. He, S.-F. Yuan, G.-Y. Yang, G.-J. Liang and Q.-M. Wang, *J. Am. Chem. Soc.*, 2020, **142**, 18086–18092.

7 M. R. Narouz, K. M. Osten, P. J. Unsworth, R. W. Y. Man, K. Salorinne, S. Takano, R. Tomihara, S. Kaappa, S. Malola, C. T. Dinh, J. D. Padmos, K. Ayoo, P. J. N. M. Garrett, J. H. Horton, E. H. Sargent, H. Häkkinen, T. Tsukuda and C. M. Crudden, *Nat. Chem.*, 2019, **11**, 419–425.

8 H. Li, P. Wang, C. Zhu, W. Zhang, M. Zhou, S. Zhang, C. Zhang, Y. Yun, X. Kang, Y. Pei and M. Zhu, *J. Am. Chem. Soc.*, 2022, **144**, 23205–23213.

9 R. Jin, C. Zeng, M. Zhou and Y. Chen, *Chem. Rev.*, 2016, **116**, 10346–10413.

10 Z. Lei, X.-K. Wan, S.-F. Yuan, Z.-J. Guan and Q.-M. Wang, *Acc. Chem. Res.*, 2018, **51**, 2465–2474.

11 A. V. Zhukhovitskiy, M. J. MacLeod and J. A. Johnson, *Chem. Rev.*, 2015, **115**, 11503–11532.

12 R. P. Herrera and M. C. Gimeno, *Chem. Rev.*, 2021, **121**, 8311–8363.

13 Y. Li and R. Jin, *J. Am. Chem. Soc.*, 2020, **142**, 13627–13644.

14 W. Dong, F. Zhang, T. Li, Y. Zhong, L. Hong, Y. Shi, F. Jiang, H. Zhu, M. Lu, Q. Yao, W. Xu, Z. Wu, X. Bai and Y. Zhang, *J. Am. Chem. Soc.*, 2024, **146**, 22180–22192.

15 Y. Li, T. Higaki, X. Du and R. Jin, *Adv. Mater.*, 2020, **32**, e1905488.

16 W. Xu, E. Wang and X. Zeng, *Acc. Mater. Res.*, 2024, **5**, 1134–1145.

17 S. Li, N.-N. Li, X.-Y. Dong, S.-Q. Zang and T. C. W. Mak, *Chem. Rev.*, 2024, **124**, 7262–7378.

18 H. Li, X. Kang and M. Zhu, *Acc. Chem. Res.*, 2024, **57**, 3194–3205.

19 C. M. Aikens, *Acc. Chem. Res.*, 2018, **51**, 3065–3073.

20 A. Ghosh, O. F. Mohammed and O. M. Bakr, *Acc. Chem. Res.*, 2018, **51**, 3094–3103.

21 K. Kwak and D. Lee, *Acc. Chem. Res.*, 2019, **52**, 12–22.

22 Y. Li, M. J. Cowan, M. Zhou, T.-Y. Luo, Y. Song, H. Wang, N. L. Rosi, G. Mpourmpakis and R. Jin, *J. Am. Chem. Soc.*, 2020, **142**, 20426–20433.

23 M. Zhou, T. Higaki, G. Hu, M. Y. Sfeir, Y. Chen, D.-E. Jiang and R. Jin, *Science*, 2019, **364**, 279–282.

24 Y. Negishi, T. Nakazaki, S. Malola, S. Takano, Y. Niihori, W. Kurashige, S. Yamazoe, T. Tsukuda and H. Häkkinen, *J. Am. Chem. Soc.*, 2015, **137**, 1206–1212.

25 T. Higaki, M. Zhou, K. J. Lambright, K. Kirschbaum, M. Y. Sfeir and R. Jin, *J. Am. Chem. Soc.*, 2018, **140**, 5691–5695.

26 C. Zeng, Y. Chen, K. Kirschbaum, K. J. Lambright and R. Jin, *Science*, 2016, **354**, 1580–1584.

27 L. Xiong and Y. Pei, *J. Phys. Chem. C*, 2021, **125**, 20670–20675.

28 M. Zhou, T. Higaki, Y. Li, C. Zeng, Q. Li, M. Y. Sfeir and R. Jin, *J. Am. Chem. Soc.*, 2019, **141**, 19754–19764.

29 E. Hulkko, O. Lopez-Acevedo, J. Koivisto, Y. Levi-Kalisman, R. D. Kornberg, M. Pettersson and H. Häkkinen, *J. Am. Chem. Soc.*, 2011, **133**, 3752–3755.

30 T. Higaki, C. Liu, M. Zhou, T. Y. Luo, N. L. Rosi and R. Jin, *J. Am. Chem. Soc.*, 2017, **139**, 9994–10001.

31 S. Chen, T. Higaki, H. Ma, M. Zhu, R. Jin and G. Wang, *ACS Nano*, 2020, **14**, 16781–16790.

32 C. Zeng, C. Liu, Y. Chen, N. L. Rosi and R. Jin, *J. Am. Chem. Soc.*, 2016, **138**, 8710–8713.

33 G. Li, C. Zeng and R. Jin, *J. Am. Chem. Soc.*, 2014, **136**, 3673–3679.

34 P. R. Nimmala and A. Dass, *J. Am. Chem. Soc.*, 2014, **136**, 17016–17023.

35 L. Luo, Z. Liu, J. Kong, C. G. Gianopoulos, I. Coburn, K. Kirschbaum, M. Zhou and R. Jin, *Proc. Natl. Acad. Sci. U. S. A.*, 2024, **121**, e2318537121.

36 Y. Chen, C. Zeng, C. Liu, K. Kirschbaum, C. Gayathri, R. R. Gil, N. L. Rosi and R. Jin, *J. Am. Chem. Soc.*, 2015, **137**, 10076–10079.

37 X. Du, X. Zhang, H. Ma, M. Zhou, T. Higaki, G. Wang, H. Wang and R. Jin, *ChemElectroChem*, 2024, **11**, e202300528.

38 S. Mustalahti, P. Myllyperkiö, T. Lahtinen, S. Malola, K. Salorinne, T.-R. Tero, J. Koivisto, H. Häkkinen and M. Pettersson, *J. Phys. Chem. C*, 2015, **119**, 20224–20229.

39 Y. Chen, C. Zeng, D. R. Kauffman and R. Jin, *Nano Lett.*, 2015, **15**, 3603–3609.

40 C. Zeng, Y. Chen, K. Kirschbaum, K. Appavoo, M. Y. Sfeir and R. Jin, *Sci. Adv.*, 2015, **1**, e1500045.

41 K. Iida, M. Noda and K. Nobusada, *J. Phys. Chem. C*, 2016, **120**, 2753–2759.

42 M. Zhou, X. Du, H. Wang and R. Jin, *ACS Nano*, 2021, **15**, 13980–13992.

43 W. Zhang, J. Kong, Y. Li, Z. Kuang, H. Wang and M. Zhou, *Chem. Sci.*, 2022, **13**, 8124–8130.

44 W. R. Jeffries, S. Malola, M. A. Tofanelli, C. J. Ackerson, H. Häkkinen and K. L. Knappenberger Jr., *J. Phys. Chem. Lett.*, 2023, **14**, 6679–6685.